

# Probabilistic pounding analysis of high-pier continuous rigid frame bridge with actual site conditions

Hongyu Jia<sup>1,2a</sup>, Jingang Zhao<sup>\*3</sup>, Xi Li<sup>1,2b</sup>, Lanping Li<sup>1c</sup> and Shixiong Zheng<sup>1d</sup>

<sup>1</sup>Department of Civil Engineering, Southwest Jiaotong University, Chengdu 610031, China

<sup>2</sup>The Key Laboratory of Urban Security and Disaster Engineering, Beijing University of Technology, Beijing 100124, China

<sup>3</sup>College of Civil Engineering, Guizhou University, Guiyang 550025, China

(Received February 18, 2018, Revised May 14, 2018, Accepted May 17, 2018)

**Abstract.** This paper studied the probability of pounding occurred between decks and abutments of a long span high-pier continuous rigid frame bridge subjected to ground motions with local soil effect. A pounding probability analysis methodology has been proposed using peak acceleration at bedrock as intensity measure (IM) for multi-support seismic analysis. The bridge nonlinear finite element (FE) models was built with four different separation distances. Effect of actual site condition and non-uniform spatial soil profiles on seismic wave propagating from bedrock to ground surface is modelled. Pounding probability of the high-pier bridge under multi-support seismic excitations (MSSE) is analyzed based on the nonlinear incremental dynamic analysis (n-IDA). Pounding probability results under uniform excitations (UE) without actual local site effect are compared with that under MSSE with site effect. The study indicates that the required design separation length between deck and abutment under uniform excitations is larger than that under MSSE as the peak acceleration at bedrock increases. As the increase of both separation distance between deck and abutment and the peak acceleration, the probability of pounding occurred at a single abutment or at two abutments simultaneously under MSSE is less than that under UE. It is of great significance considering actual local site effect for determining the separation distance between deck and abutment through the probability pounding analysis of the high-pier bridge under MSSE.

**Keywords:** local soil site effect; separation distance; pounding probability; high-pier bridge; nonlinear incremental dynamic analysis

## 1. Introduction

A majority of superstructure damages of bridges located in seismic prone regions are relevant to the pounding between adjacent decks and deck to abutment under strong ground motions (Bi *et al.* 2010, Bi *et al.* 2012). More and more bridge superstructure pounding has been observed in almost all the recent major earthquakes worldwide (Hao 1998, Kawashima *et al.* 2009). Particularly, in the southwestern mountainous regions of China surrounding by the Pacific Rim and Eurasian Seismic Belts, an increasing number of high-pier bridges have been built as a result of demanding development for both roadway and railway transportation network (Jia *et al.* 2013). It is known that the stiffness of high-pier bridges is usually smaller than that of the generic bridges due to the higher slender piers, thereby

larger relative displacement between adjacent girders and deck to abutment of high-pier bridges will be induced under earthquakes (Wang *et al.* 2010, Zhang *et al.* 2014). The pounding of bridge structures in mountainous regions can result in the pull-off-and-drop collapse of their decks and other damages of the deck, abutment, bearing, side block etc. (Bi and Hao 2013). The high-pier bridges in mountainous area are usually very critical components within the transportation network, and once the bridges were collapsed, the local transportation system will be destroyed and the robustness of seismic evacuation and rescue will be significantly compromised (Chen and Zheng 2015, Yin *et al.* 2011). Therefore, study on seismic pounding for high-pier bridges becomes much more essential for the western mountainous regions than that in the plain districts.

The poundings on high-pier bridges under earthquakes are produced due to the out-of-phase movements between adjacent high-pier bridge segments by different dynamic characteristics of adjacent bridge segments, spatially varying seismic excitations in mountainous area, various local site conditions, and soil-structure interaction (SSI) effect (Sharmin *et al.* 2017, Gou *et al.* 2013, Gou *et al.* 2015). In the mountainous area, the local soil layers underneath each bridge pier is significantly variable owing to the complicated terrain structures. The seismic surveys from many past earthquakes concluded that the distribution and properties of local soil layers have a significant impact

\*Corresponding author, Assistant Professor

E-mail: zhaojingangtumu@163.com

<sup>a</sup>Associate Professor

E-mail: Hongyu1016@swjtu.edu.cn

<sup>b</sup>Assistant Professor

E-mail: Xi.Li@swjtu.edu.cn

<sup>c</sup>Assistant Professor

E-mail: Lilanping@swjtu.edu.cn

<sup>d</sup>Professor

E-mail: zhengsx@swjtu.edu.cn

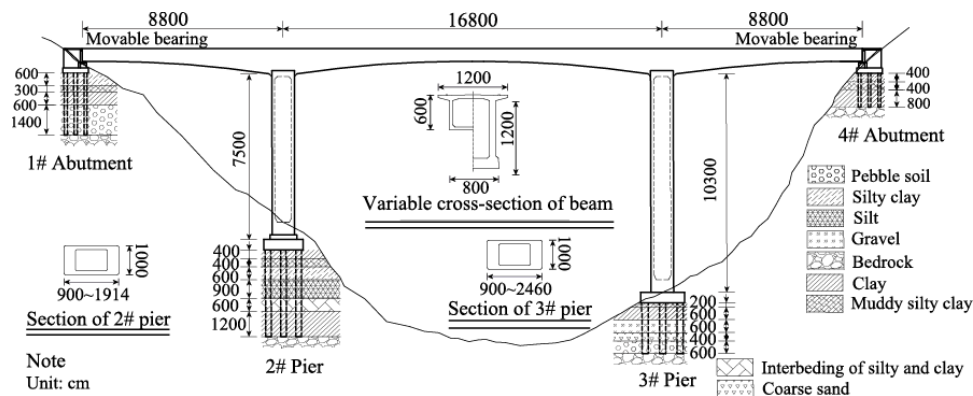


Fig. 1 Layout of the high pier bridge

on the seismic responses of large-scale structures (Kawashima *et al.* 1996, Lin *et al.* 2008). The influence stems mainly from the fact that the site soil layer filters seismic waves propagating from bedrock up to the ground and varying local soil condition will induce different amplitude and phase of ground seismic waves, thereby resulting in significant different bridge responses.

Most of the studies on bridge poundings are based on the deterministic dynamic methods (e.g., the single-degree-of-freedom (SDOF) or multiple-degree-of-freedom (MDOF) models) and very few were devoted to investigate the influence of local soil layers on pounding of high-pier bridges in mountainous regions (Beilic *et al.* 2017, Beneldjouzi *et al.* 2017). Ruangrassamee and Kawashima investigated the relative displacement spectra for pounding of bridge systems as modelled by two colliding SDOF system (Ruangrassamee 2001). Pounding effects on seismic response of multi-frame bridge structures were also studied by using a simplified lumped mass model (DesRoches *et al.* 2002). Chouw and Hao studied the influence of spatially varying ground motions and soil-structure interaction on the relative displacement responses of two bridge frames (Chouw *et al.* 2008a, Chouw *et al.* 2008b, Hao *et al.* 2008). Hao *et al.* (1998) investigated the required seating length to prevent the pull-off-and-drop collapse of bridge decks. A parametric investigation of the pounding response of multi-span simply supported bridges was performed by Zanardo *et al.* (2002).

Moreover, detailed analyses were performed for bridge structure pounding with the aid of finite element method (FEM). The pounding mitigation techniques were developed based on the FEM with the superstructure segments and piers modelled as elastic beam-column elements (Jankowski *et al.* 1998). Chouw *et al.* studied the influence of multi-side collisions on bridge response (with girders and pier modelled as beam-column elements) due to ground motion spatial variations (Hao *et al.* 2008). Bi *et al.* investigated the influence of ground motion spatial variation, site condition and SSI on the required separation distances of bridge structures to avoid seismic pounding (Bi *et al.* 2011). The detailed three-dimensional FEM nonlinear pounding analysis of the bridge under spatially varying ground motions was conducted by Bi and Hao (2013). A 3-span simply-supported steel bridge is used to investigate the earthquake-induced pounding effects on bridge piers using

a simplified idealized analytical model and it revealed that the size of separation distance depends on the nonlinearity of bridge piers significantly (Won *et al.* 2015).

Following the aforementioned discussions, probabilistic pounding analysis of bridges under different seismic intensities is limited, especially for the probability-based approaches on required pounding separation distance. In addition, in the probabilistic pounding analysis of bridges under non-uniform ground motions with a series of seismic intensities, it is essential to determine a unique IM for bottom base of bridge piers (with varying seismic inputs) to achieve consistent engineering demand parameter (EDP), e.g., the required separation distance (Jeon *et al.* 2015).

This paper has developed a probability-based pounding analysis methodology for bridges under spatially varying ground motions, by taking the peak ground motions at bedrock as a constant IM for multi-support seismic analysis. The spatial variability of ground motions is considered herein, but the limitation is made in the range of local site effect in the paper. The probability of pounding occurred between decks and abutments of the high-pier long-span continuous rigid bridge has been studied considering effect of local soil layers. Section 2 presents the FEM of a high-pier bridge and the fundamental theory of bridge pounding. Section 3 modeled the seismic wave on bedrock and effects of local soil layer. In Section 4, the nonlinear probability analysis process is presented based on the software OpenSEES. The probability distribution model of peak relative displacement between deck and abutment and demand of the required separation distance were discussed. And the proposed probabilistic pounding analysis methodology was demonstrated by employing a high pier bridge. Conclusions and observations were drawn in Section 5.

## 2. Finite element model and theory of pounding

To study the influence of practical local soil layers on the dynamic response of high-pier bridges under spatially varying ground motions, a prestressed concrete rigid frame bridge, with the span layout of 88 m+168 m+88 m and the pier heights of 75 m and 103 m at piers #2 and #3, respectively, are used and presented in Fig. 1. The bridge has a single-box single cell girder having a variable

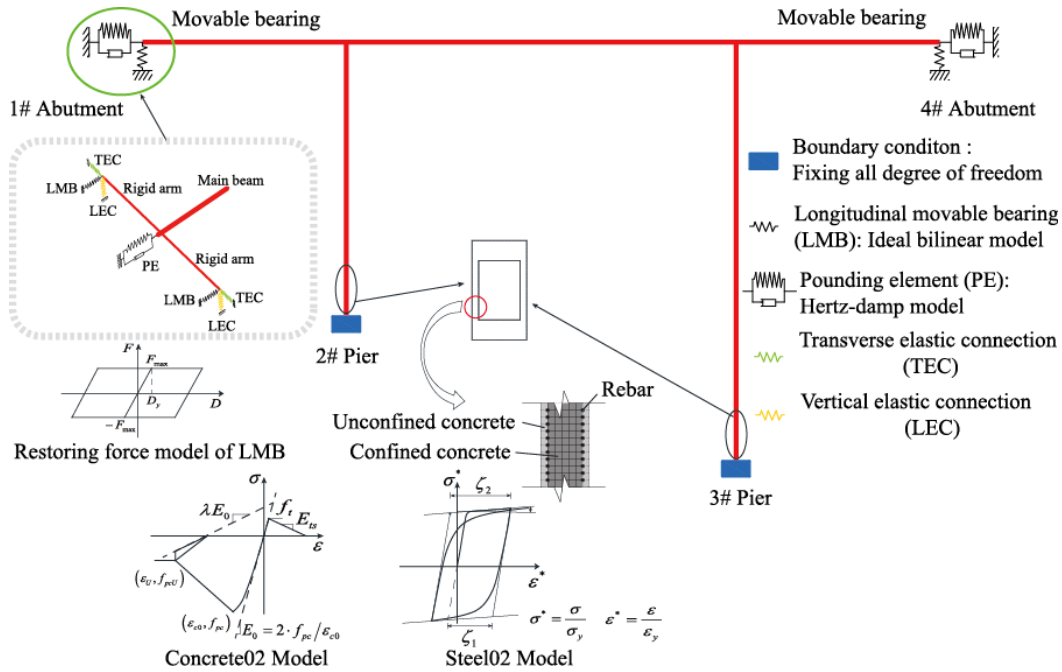


Fig. 2 FE model of the high-pier bridge

parabolic cross-section height and a top width of 12 m and bottom width of 8 m. All the piers have thin-wall and variable rectangle sections.

Based on the nonlinear FEM software OpenSEES, the numerical model of the high-pier bridge was built in Fig. 2 for pounding probability analysis with actual local soil condition. The seismic damages of high-pier bridges frequently occurred on the bridge piers while the girder of such bridge mostly remain elastic. The Displacement-Based Beam-Column Element (DBE) and Elastic Section (ES) are used to model main girder. The variable section of main girder is modeled by assigning different section parameters at both ends of the element. Force-Based Beam-Column Element (FBE) and Fiber Section (FS) are adopted to model the elastic-plastic behavior of bridge piers. The main deck is constrained in the transverse direction owing to the lateral displacement-limiting device installed between deck and piers, and it is assumed that the collision occurred in the longitudinal direction of the bridge. The bottom of all piers are fixed and the bearing is modeled using the Link Elements (LE) which connects two nodes of bearing end. The element can have zero or non-zero length and have 1 to 6 degrees of freedom, where only the transverse and rotational degrees of freedom are coupled as long as the element has non-zero length. Yet only the transverse degree of freedom is considered herein. The Bilinear Hysteretic Material is used to model the nonlinear behavior of bearing sliding with the model parameters in accordance with the China national seismic design guideline of highway bridges. Some parameters are given such as longitude stiffness of all bearings: 47911 (kN/m), yield stress or force: 191.644 (kN), isotropic hardening Modulus:  $10^{-6}$  and kinematic hardening Modulus:  $10^{-6}$ . The confined and unconfined concrete are both modeled by Concrete02 Element with the material parameters given by Zhao *et al.* (2017). The steel material is modeled by the Steel02 Element.

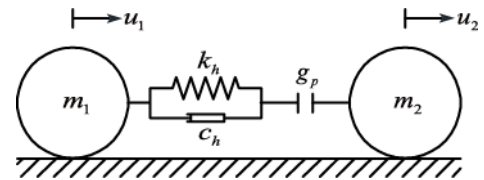


Fig. 3 Analysis model of structural pounding

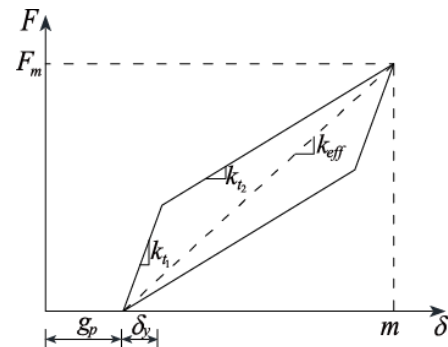


Fig. 4 Hertz-damp model

The impact between two adjacent decks and between deck and abutment of high-pier bridges under earthquakes is a complicated dynamic problem. A wide range of modelling techniques are investigated to analyze the pounding of bridges to reduce the bridge damages and these methods have their own merits and demerits. The Hertz-damp model (HDM), shown in Fig. 3, is used to model the pounding of bridges occurring between girder and abutment in this paper. The nonlinear spring and nonlinear damper in the HDM are combined to model, respectively, the stiffness and energy dissipation in the pounding process. For practical simplification, the HDM is usually transformed into a bilinear stiffness contact model and the relationship between pounding force and displacement is given in Fig. 4 with the equation as

$$F = \begin{cases} k_h (u_1 - u_2 - g_p)^n + c_h v & u_1 - u_2 - g_p \geq 0 \\ 0 & u_1 - u_2 - g_p < 0 \end{cases} \quad (1)$$

in which  $k_h$  and  $c_h$  are pounding stiffness and damping coefficients, respectively. Typically the value of  $k_h$  is considered as the axial stiffness ( $EA/L$ ) of main decks (Maison *et al.* 1990, Maison *et al.* 1992);  $u_1, u_2$  denote the displacements of two adjacent pounding segments; the separation gap size between deck and abutment is expressed as  $g_p$ ; and  $n$  is the Hertz model coefficient commonly equaling to 3/2.

Assuming that the maximal pounding force in HDM and the bilinear model of Fig. 4 are equal, the equivalent stiffness  $k_{eff}$  can be derived as

$$k_{eff} = k_h \sqrt{\delta_m} \quad (2)$$

where  $\delta_m$  represents the maximum intrusion displacement on the contact surface. Alternatively, the equivalent stiffness  $k_{eff}$  can be expressed as

$$k_{eff} \delta_m = k_{t_1} \delta_y + k_{t_2} (\delta_m - \delta_y) \quad (3)$$

in which  $\delta_y$  denotes the yield displacement, and  $k_{t_1}$  and  $k_{t_2}$  are initial stiffness and strain strengthening stiffness, respectively.

Therefore, the area enclosed by the impact force and displacement curve can be derived as

$$A_m = (k_{t_1} - k_{t_2}) \delta_y (\delta_m - \delta_y) \quad (4)$$

The dissipation energy  $\Delta E$  in the pounding process can be additionally obtained as

$$\Delta E = \frac{k_h \delta_m^{n+1} (1 - e^2)}{n+1} \quad (5)$$

Table 1 Properties of simplified Hertz-damp model

Parameters	Values
Pounding stiffness $k_h$	868 kN/mm <sup>3/2</sup>
Hertz coefficient $n$	3/2
Recovery coefficient $e$	0.8
Maximal intrusion displacement $\delta_m$	16 mm
Yield coefficient $a$	0.1
Yield displacement $\delta_y$	1.6 mm
Equivalent stiffness $k_{eff}$	3472 kN/mm
Initial stiffness $k_{t_1}$	8472 kN/mm
Strain strengthening stiffness $k_{t_2}$	2916 kN/mm

in which  $e$  is a recovery coefficient with a value generally in the range of 0.6 to 0.8.

The relationship between yield displacement  $\delta_y$  and the maximum intrusion displacement  $\delta_m$  is given by

$$\delta_y = a \delta_m \quad (6)$$

where  $a$  is the yield coefficient with a value of 0.1. During the impact process, the dissipation energy  $\Delta E$  equal the value of enclosed area formed by the impact force and displacement curve, namely  $A_m = \Delta E$ . Based on Eqs. (1)-(6), one can obtain

$$\begin{cases} k_{t_1} = k_{eff} + \frac{\Delta E}{a \delta_m^2} \\ k_{t_2} = k_{eff} - \frac{\Delta E}{(1-a) \delta_m^2} \end{cases} \quad (7)$$

According to Eq. (7), once the pounding stiffness  $k_h$ , recovery coefficient  $e$ , maximal intrusion displacement  $\delta_m$ , and yield coefficient  $a$  are determined, one can obtain all HDM parameters as listed in Table 1.

Table 2 Selected bedrock seismic records

No.	Location	Station	Date	Site type	$V_{s30}$ (m/sec)	Magnitude	Epical distance (km)	PGA (g)
1	Chi-Chi	HWA003	1999	A	1525.85	7.62	56.14	0.138
2	Chi-Chi	ILA001	1999	B	909.09	7.62	103.20	0.025
3	Chi-Chi	ILA063	1999	B	996.51	7.62	61.06	0.095
4	Chi-Chi	TAP077	1999	B	1022.77	7.62	119.00	0.034
5	Chi-Chi	TCU085	1999	B	999.66	7.62	58.09	0.063
6	Chi-Chi	CHY102	1999	B	804.36	6.20	39.30	0.059
7	Chi-Chi	TAP065	1999	B	1023.45	7.62	122.48	0.038
8	Niigata	FKSH07	2004	B	828.95	6.63	52.30	0.143
9	Niigata	TCGH17	2004	B	1432.75	6.63	77.50	0.065
10	Iwate	AKTH05	2008	B	829.46	6.90	39.41	0.085
11	Hector Mine	LA-Griffith Park Observatory	1999	B	1015.88	7.13	185.92	0.018
12	Loma Prieta	SF-Rincon Hill	1989	B	873.10	6.93	74.14	0.093
13	Loma Prieta	Piedmont Jr High School Grounds	1989	B	895.36	6.93	73.00	0.084
14	San Fernando	Pasadena-Old Seismo Lab	1971	B	969.07	6.61	21.50	0.205
15	Northridge-01	Vasquez Rocks Park	1994	B	996.43	6.69	23.64	0.151
16	Northridge-01	LA-Wonderland Ave	1994	B	1222.52	6.69	20.29	0.159
17	Northridge-01	Pacoima Dam (downstr)	1994	A	2016.13	6.69	7.01	0.434
18	Loma Prieta	Gilroy Array #1	1989	B	1428.14	6.93	9.64	0.485
19	Loma Prieta	Los Gatos-Lexington Dam	1989	B	1070.34	6.93	5.02	0.443
20	Tabas_Iran	Tabas	1978	B	766.77	7.35	2.05	0.862

### 3. Selection of bedrock seismic wave and local soil effects

#### 3.1 Selection of bedrock seismic waves

To account for the local site effect on the dynamic analysis of high-piers bridges, bedrock seismic waves are needed. The bedrock material is defined as the one having a shear velocity more than 750 m/sec in accordance to USGS site classification specification. A total of 20 bedrock seismic waves are selected from PEER ground motion database and these ground motions (PEER 2005) are listed in Table 2. As seen from Table 2, the selected bedrock seismic waves have the moment magnitude ranging from 6.20 to 7.62 and the peak and minimum ground accelerations of 0.862 g and 0.018 g, respectively. Consequently, the selected seismic records consist of large, medium and small earthquakes. The absolute acceleration response spectrum with a damping ratio of 5% and PGA of 1.0 g is shown in Fig. 5.

#### 3.2 Modelling of local soil layer effects

During an earthquake, the seismic wave travelling from the bedrock to ground through soil layers results in the alternating stress in soil profile due to the amplification and filtration effects of soil layers. The resulting soil nonlinearity will affect the peak acceleration and frequency spectrum characteristics of seismic wave (Li *et al.* 2001).

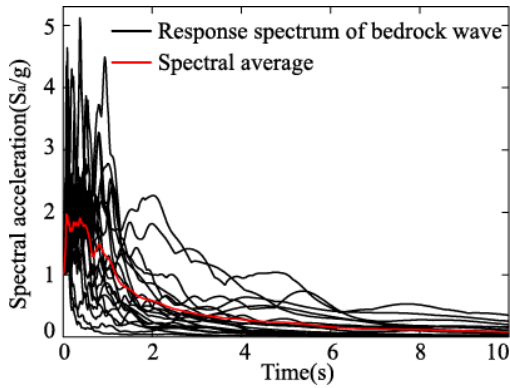


Fig. 5 Response spectra of seismic waves at bedrock

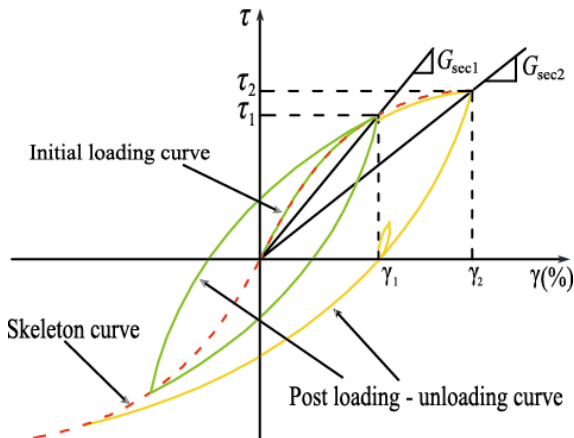


Fig. 6 Hyperbolic constitutive model

Hence, the local site effects and non-uniform spatial soil distribution should be modeled for a more reasonable and realistic ground motion input in seismic analysis of high-pier bridges. The acceleration seismic waves taking into account the filtration of soil layers will be transformed into displacement seismic waves, because the displacement seismic waves are applied to the bottom base of piers and abutments by using the commands of pattern MultipleSupport \$pattern Tag in OpenSEES software for the dynamical analysis of bridge structures subjected to multi-support excitations. The frequency-domain equivalent linearization method and time-domain direct integration method are widely used to account for the local soil layer effect. The time-domain direct integration method has advantages over the frequency-domain equivalent linearization method in modelling the soil fundamental dynamic behaviors such as the nonlinearity, hysteresis, and residual strain accumulation. Among the time-domain direct integration methods, the modified hyperbolic constitutive model proposed by Matasovic is adopted (Matasovic *et al.* 1993). The initial skeleton curve has the following equation and is shown in Fig. 6

$$\tau = \frac{\gamma G_{mo}}{1 + \beta (\gamma / \gamma_{\tau})^s} \quad (8)$$

in which  $\tau$  is the shear stress,  $G_{mo}$  denotes the initial shear modulus,  $\gamma$  represents the known shear strain,  $\gamma_{\tau}$  is the reference shear strain, and both  $\beta$  and  $s$  are soil filtration parameters.

The reference shear strain  $\gamma_{\tau}$  can be obtained by the following Eq. (9)

$$\gamma_{\tau} = REF.strain \left( \frac{\sigma_v}{REF.stress} \right)^b \quad (9)$$

where  $\sigma_v$  is the vertical effective stress,  $REF.strain$  and  $REF.stress$  are reference effective strain and stress, respectively. Typically,  $REF.stress=0.18\text{MPa}$  and  $b$  denotes the model regression parameters. The small strain damping of  $\lambda$  is obtained as

$$\lambda = Dampingratio \left( \frac{1}{\sigma_v} \right)^d \quad (10)$$

where both  $Dampingratio$  and  $d$  are model fitting parameters.

For simplicity, effect of pore water pressure of soil on the dynamic local soil effect is ignored and the Masing method is used to construct the soil hysteretic model. Based on the modified hyperbolic constitutive model, parameters including  $Dampingratio$ ,  $REF.stress$ ,  $REF.strain$ ,  $\beta$ ,  $s$ ,  $b$ , and  $d$  need to be determined. These parameters are obtained by modulus reduction and damping curve fitting procedure (MRD) to comprehensively consider the influence of variation of shear modulus curve ( $G/G_{max}-\gamma$ ) and damping ratio curve ( $\lambda-\gamma$ ). Based on the realistic soil conditions of Fig. 1 at the sites of #1 abutment, #2 pier, #3 pier and #4 abutment and the geotechnical properties of Table 4, all the information of soil layers at practical sites of selected high-pier bridge are derived and presented in Table 5 (Yousef *et al.* 2004).

Table 4 Laboratory test parameters of soils

No.	Soil layer	Shear wave velocity (m/s)	Density (kg/m <sup>3</sup> )
1	Silty clay	150	1950
2	Muddy silty clay	88	1850
3	Clay	190	1950
4	Silt	160	2010
5	Gravel	309	2150
6	Coarse sand	256	2000
7	Pebble soil	380	2050
8	Interbedding of silty and clay	220	1950

Table 5 Nonlinear parameters of soils

No.	Name	Parameter	Shear wave velocity $r_d \times 10^{-4}$							
			0.05	0.1	0.5	1	5	10	50	100
1	Silty clay	$G/G_{\max}$	0.994	0.988	0.943	0.892	0.622	0.452	0.241	0.136
		$\lambda$	0.029	0.037	0.063	0.077	0.106	0.114	0.122	0.123
2	Muddy silty clay	$G/G_{\max}$	0.860	0.790	0.600	0.470	0.165	0.090	0.015	0.010
		$\lambda$	0.030	0.035	0.055	0.077	0.137	0.165	0.220	0.235
3	Clay	$G/G_{\max}$	0.995	0.990	0.953	0.910	0.670	0.504	0.260	0.139
		$\lambda$	0.032	0.043	0.083	0.105	0.154	0.168	0.182	0.184
4	Silt	$G/G_{\max}$	0.994	0.988	0.943	0.893	0.625	0.455	0.246	0.138
		$\lambda$	0.011	0.016	0.036	0.050	0.084	0.095	0.107	0.109
5	Gravel	$G/G_{\max}$	0.993	0.985	0.924	0.858	0.544	0.374	0.107	0.056
		$\lambda$	0.004	0.005	0.021	0.031	0.074	0.094	0.124	0.129
6	Coarse sand	$G/G_{\max}$	0.965	0.935	0.775	0.660	0.300	0.250	0.105	0.090
		$\lambda$	0.006	0.010	0.030	0.045	0.088	0.103	0.124	0.130
7	Pebble soil	$G/G_{\max}$	0.990	0.970	0.900	0.850	0.700	0.550	0.320	0.200
		$\lambda$	0.004	0.006	0.019	0.030	0.075	0.090	0.110	0.120

Note:  $r_d$  is shear strain of soil,  $G/G_{\max}$  is dynamic shear modulus ratio,  $\lambda$  is the damping ratio, and interbedding of silty and clay has the same parameter as that of clay.

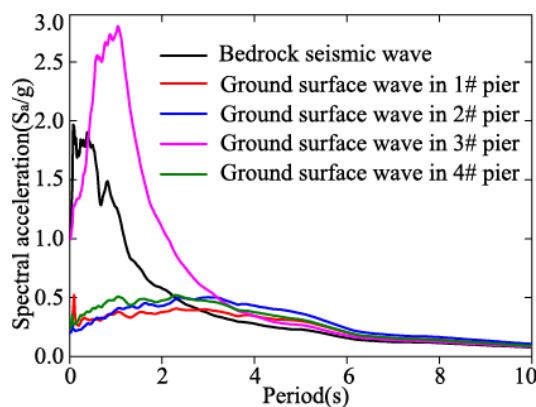


Fig. 7 Comparison of average response spectrum

In the site response analysis, each of the selected 20 bedrock seismic waves is modified into a total of 11 waves with the peak accelerations of 0.05 g, 0.1 g, 0.2 g, 0.3 g, 0.4 g, 0.5 g, 0.6 g, 0.7 g, 0.8 g, 0.9 g, and 1.0 g, respectively. Then a total of 220 seismic waves are generated and used in the time-domain nonlinear site response analysis for modelling seismic wave propagation from bedrock to ground surface through realistic local soil. For brevity, only the average response spectra of seismic waves at ground

surface and bedrock are provided in Fig. 7.

Generally, the peak average response spectrum at ground surface at pier #3 is about 1.5 times larger than that of at the bedrock; however, the peak values were de-amplified by about  $\frac{1}{4}$  times of that at bedrock at the other site locations. Because the major soil components include the pebbles, gravel and coarse sand at pier #3, the soil layer is considered to be the hard soil layer in accordance with shear wave velocity value of Table 4. It is further indicated that the predominant frequency of hard soil layer at pier #3 and the dominant frequency of bedrock seismic wave are close, resulting in the resonance that the bedrock seismic wave was amplified by about 1.5 times.

To avoid the influence of thickness of soil layer on the peak acceleration and the response spectrum, the maximum frequency of seismic waves allowed to propagate in the corresponding soil layer is used to determine the values of the thickness of soil layer. The maximum frequency can be obtained as

$$f_{\max} = V_s / 4h \quad (11)$$

in which  $V_s$  is the shear wave velocity,  $h$  denotes the thickness of soil layer, and the maximum frequency  $f_{\max}$  of arbitrary soil layer is usually required not being less than 25 Hz.

#### 4. Methodology on the probabilistic pounding analysis of bridge

##### 4.1 Analysis procedure for probabilistic pounding analysis of bridge

In the process of probabilistic pounding analysis of the employed high-pier and continuous rigid frame bridge, the following procedure are used:

- (1) Based on the FE software of OpenSEES, a total of four model samples are established with the separation length (i.e., the pounding parameter  $g_p$ ) of 0.1 m, 0.2 m, 0.3 m, and 0.4 m, respectively;
- (2) Ground seismic waves generated in Section 3.2 is applied to the base of the piers and abutments in FE model for the n-IDA of the bridge subjected to MSSE. For comparative analysis, the UE seismic analysis is also carried out by directly using the bedrock seismic waves;
- (3) Peak relative displacement between main deck and abutment is computed, respectively, based on two types of seismic excitations of MSSE and UE and statistical analysis is then performed to determine probability distribution model;
- (4) Required separation lengths under different IM of ground motions are calculated based on the probability distribution model of peak relative displacement and effects of different separation gap and effects of local soil layers on the required separation distance are studied;
- (5) Marginal pounding probability at abutments #1 and 4# and system pounding probability are derived based on the random variable of IM for bedrock seismic waves.

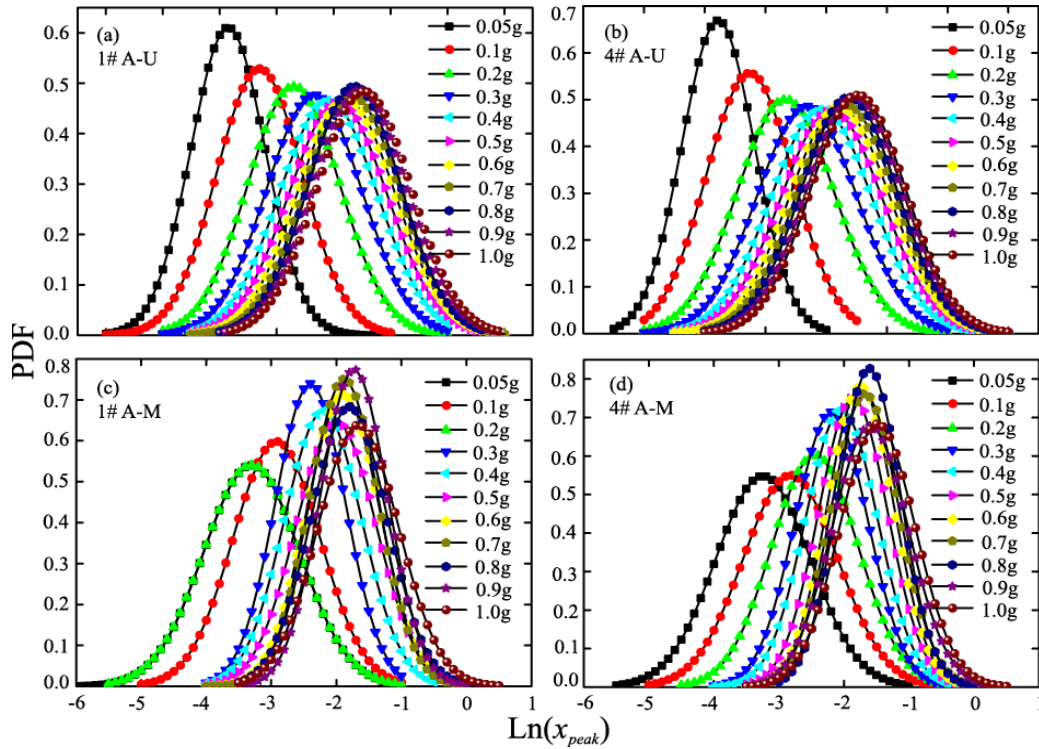


Fig. 8 Probability density function for peak relative displacement

Notes: PDF is the probability density function, *A* denotes the abutment, *U* the uniform excitation, and *M* the multi-support seismic excitation.)

#### 4.2 Probability distribution model of peak relative displacement

Under ground excitations, the peak relative displacement between abutment and end of main beam varies with the peak acceleration and spectral characteristic of the seismic waves. The peak relative displacement is usually assumed to follow the probability distribution models such as extreme value distribution, logarithmic normal distribution and normal distribution, etc. The peak relative displacement value between main deck and abutment is expressed with natural logarithm under UE and MSSE and statistical analysis is then carried out. It reveals that the natural logarithm of peak relative displacement follows the normal distribution, namely the peak relative displacement follows the lognormal distribution. For brevity, only results of required separation gap of 0.1 m is given in Fig. 8 for both UE and MSSE.

#### 4.3 Probabilistic demand analysis of required separation distance

As discussed in Section 4.2, the peak relative displacement follows lognormal distribution conditional on the peak acceleration of bedrock seismic wave. The probability density function can be derive as

$$f(x_{peak}) = \frac{1}{x_{peak} \sigma_{PGA} \sqrt{2\pi}} \exp\left(-\frac{(\ln x_{peak} - \mu_{PGA})^2}{2\sigma_{PGA}^2}\right) \quad (12)$$

where  $\mu_{PGA}$  and  $\sigma_{PGA}$  denote logarithmic mean and standard

deviation of peak relative displacement conditional on the peak acceleration *PGA* of bedrock seismic wave.

Based on properties of lognormal distribution function, the peak relative displacement within the interval having a confidence level of 99.74% can be derived as

$$\left[ \frac{\exp(\mu_{PGA})}{[\exp(\sigma_{PGA})]^3}, \exp(\mu_{PGA}) \cdot [\exp(\sigma_{PGA})]^3 \right] \quad (13)$$

Thus it is reasonable and acceptable that the upper limit of the interval can be considered as the design separation distance with an exceeding probability of 0.26%. Fig. 9 presents a comparison of design separation distance with different expansion joint widths at #1 and #4 abutments under UE and MSSE.

As described in Fig. 9, as the increase of separation width from 0.1 m to 0.4 m, the design separation distance increases under every IM of PGA. The design separation width in abutment #1 and #4 are basically similar owing to the UE; however, the results become opposite under MSSE and a maximum difference of 1 m occurs at the separation width of 0.4 m and the PGA of 0.9 g. Since, under UE, the same bedrock seismic waves are used at each pier base for every IM, asymmetric responses of the high-pier bridge are merely excited. However, under the MSSE that considering effects from local site effect and spatial non-uniform soil distribution, both asymmetric and symmetric responses of the bridge are excited and the resulting deformation is mutually offset. Therefore, the MSSE results in smaller design separation width and the UE would overestimate the demand of separation width between bridge deck and abutment.

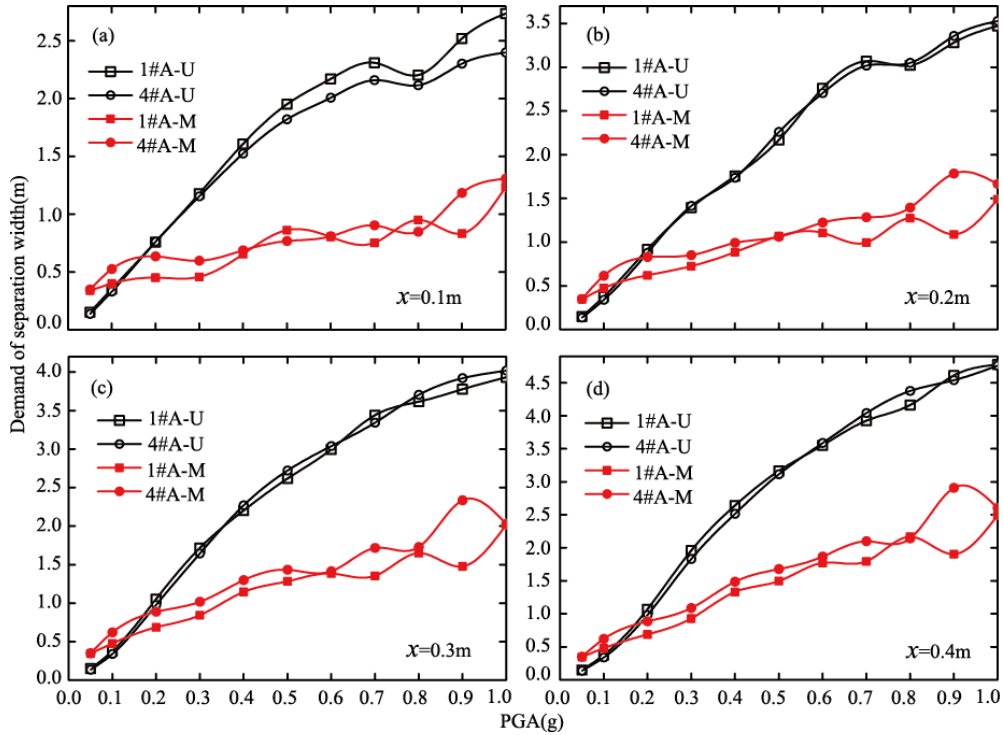


Fig. 9 Comparison of design width of expansion joint (Note: A-abutment; U-uniform excitation; M-multi-support seismic excitation; x-separation width)

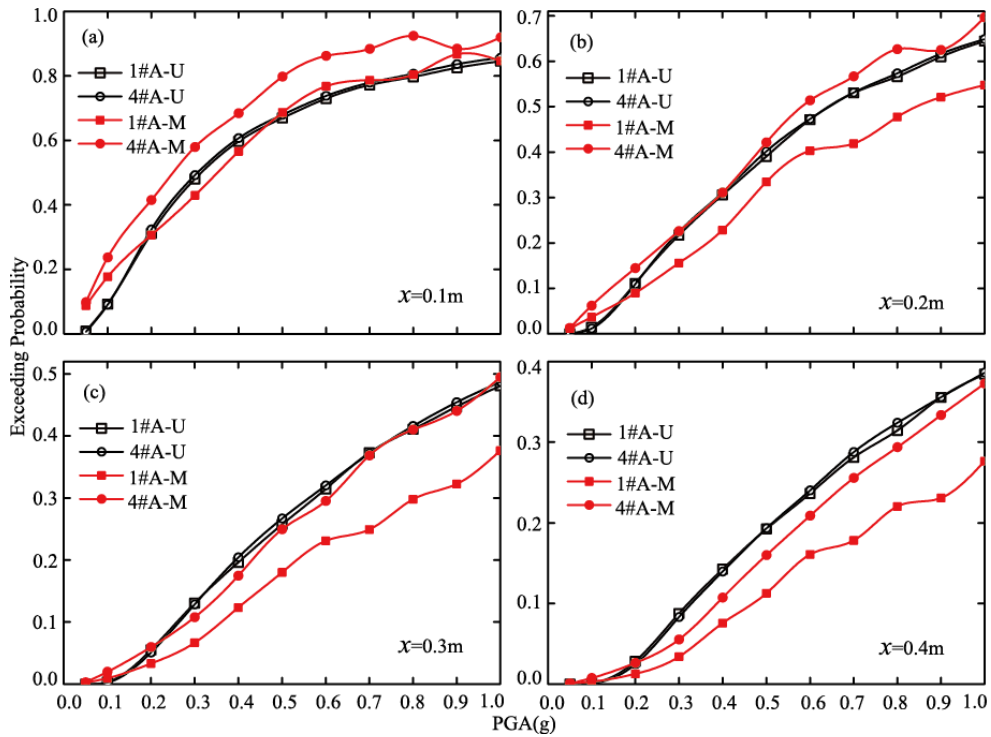


Fig. 10 Comparison of pounding probability

#### 4.4 Pounding probability analysis of a high-pier bridge

Suppose the pounding between deck and abutment is about to occur when the relative displacement response exceeds the separation gap of expansion joint, the probability of pounding under seismic IM of PGA can be expressed as

$$P(x|PGA) = 1 - \Phi\left(\frac{\ln(\Delta_i) - \mu_{PGA}}{\sigma_{PGA}}\right) \quad (14)$$

in which  $\Delta_i$  is separation width of expansion joint and  $\Phi(\square)$  denotes the standard normal distribution function.

To investigate the influence of separation width of expansion joint and local soil layer effect on the pounding

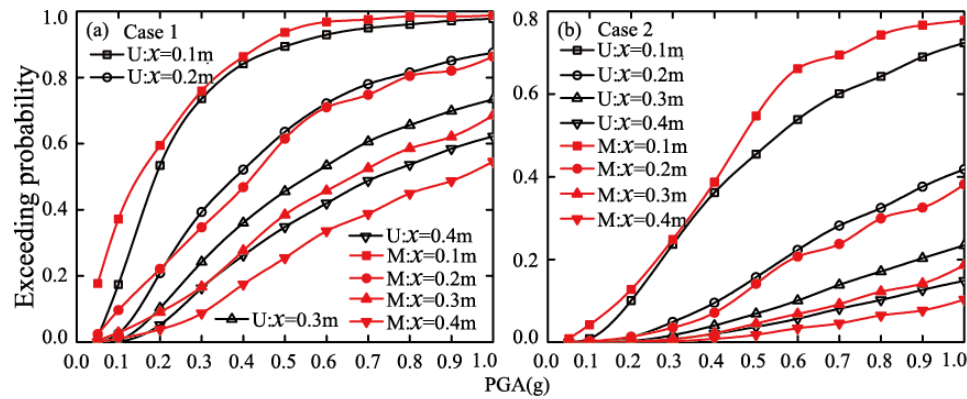


Fig. 11 Comparison of system pounding probability

probability, the pounding probability between deck and abutment under both UE and MSSE are presented in Fig. 10 for various separation distance. Assuming that the pounding incidence between #1 and #4 abutments are independent, the following two cases of system pounding probability are calculated and are presented in Fig. 11 (Jia *et al.* 2018).

(1) Case 1: at least one pounding event occurred in #1 and #4 abutments;

Case 2: pounding events occurred simultaneously in #1 and #4 abutments.

As shown in Fig. 10, the pounding probability in #1 abutment agrees with that of abutment #4 under UE but exhibit evident difference under MSSE. The pounding probability in #4 abutment is larger than that of #1 since #4 abutment is close to the highest pier #3. Additionally the uniform rule of the influence of the MSSE caused by the filtration action of soil layers on the pounding probability fails almost to be obtained, so specific problem of pounding of high-pier bridges will need specially to be analyzed in detail. For instance, as the increase of the separation width from 0.1 m to 0.4 m, the pounding probability gradually decreases. When expansion joint width equals 0.1 m, the pounding probability in abutment #1 under MSSE is greater than that under UE. As the increase of expansion joint width, the pounding probability in abutment #1 under MSSE is less than that under UE. When the expansion joint width equaling 0.4 m and the PGA exceeding 0.2 g, the probability of pounding in #1 abutment under MSSE is completely less than that under UE. The pounding probability in #4 abutment under MSSE is partially greater than that under UE. When the expansion joint width exceeding 0.2 m and the PGA exceeding 0.2 g, the pounding probability occurs in #4 abutment under MSSE is less than that under UE.

The system pounding probability in Case 1 is greater than that in Case 2, as observed from Fig. 11. With an expansion joint width of 0.1 m, the system pounding probability in Cases 1 and 2 owing to MSSE is higher than that under UE. However, when the expansion joint width beyond 0.2 m and the PGA exceeding 0.2 g, the system pounding probability in Cases 1 and 2 under MSSE is less than that under UE. In Case 1, there is a maximum difference of 0.06 between system probability between MSSE and UE, and the maximum difference value of 0.1 in Case 2.

## 5. Conclusions

A long-span high-pier continuous rigid frame bridge is employed for the probabilistic pounding analysis. The nonlinear FE models with different width of expansion joint was developed to investigate actual local site effect on pounding between bridge segments. The analysis results of the bridge under MSSE and UE are compared and the following conclusion were drawn:

- This paper has proposed a probability pounding analysis method utilizing the peak acceleration of bedrock as the seismic IM for multi-support dynamic analysis;
- Under the same IM of PGA on bedrock, the peak relative displacement between deck and abutment under both the UE and the MSSE follow the lognormal distribution;
- The required design separation distance was overestimated largely under UE and the MSSE analysis considering actual local site effect is recommended in probabilistic analysis of separation gap between bridge segments;
- The pounding probability in #1 abutment agree with that for abutment #4 under UE but with completely different pounding probabilities under MSSE. The pounding probability under MSSE is generally less than that under UE;

With the increase of width of expansion joint and the PGA of bedrock, the system pounding probability in Cases 1 and 2 is less than that under UE due to local site effect.

## Acknowledgments

The research was supported by the National Science Foundation of China under Grant No. 51308465 and the Postdoctoral Science Foundation of China under Grant No. 2015M580031. The research was also partially supported by Open Research Subject of Key Laboratory of Green Building and Energy Conservation of Sichuan Province (Grant No. szjj2016-096), the Scientific Research Foundation for Introduced Talent of Guizhou University under Grant No. 201517, the Doctoral Scientific Research Foundation of Liaoning Province under Grant No. 20170520201, the first class subject foundation of Civil

Engineering of Guizhou Province under Grant No. QYNYL[2017]0013, and the Doctoral Scientific Research Foundation of Liaoning Province under Grant No. 20170520201.

## References

- Ates, S., Bayraktar, A. and Dumanoglu, A.A. (2006), "The effect of spatially varying earthquake ground motions on the stochastic response of bridges isolated with friction pendulum systems", *Soil Dyn. Earthq. Eng.*, **26**(1), 31-44.
- Beilic, D., Casotto, C., Nascimbene, R., Cicola, D. and Rodrigues, D. (2017), "Seismic fragility curves of single storey RC precast structures by comparing different Italian codes", *Earthq. Struct.*, **12**(3), 359-374.
- Beneldjouzi, M., Laouami, N. and Slimani, A. (2017), "Numerical and random simulation procedure for preliminary local site characterization and site factor assessing", *Earthq. Struct.*, **13**(1), 79-87.
- Bi, K., Hao, H. and Chouw, N. (2010), "Required separation distance between decks and at abutments of a bridge crossing a canyon site to avoid seismic pounding", *Earthq. Eng. Struct. D.*, **39**(3), 303-323.
- Bi, K., Hao, H. and Chouw, N. (2011), "Influence of ground motion spatial variation, site condition and SSI on the required separation distances of bridge structures to avoid seismic pounding", *Earthq. Eng. Struct. D.*, **40**(9), 1027-1043.
- Bi, K. and Hao, H. (2013), "Numerical simulation of pounding damage to bridge structures under spatially varying ground motions", *Eng. Struct.*, **46**, 62-76.
- Chen, H. and Zheng, S.X. (2015), "Seismic response of ultra high-pier railway bridge under spatially varying site conditions of earthquake excitations", *J. Highw. Tran. Res. Devel.*, **9**(2), 61-68.
- DesRoches, R. and Muthukumar, S. (2002), "Effect of pounding and restrainers on seismic response of multi-frame bridges", *J. Struct. Eng.*, ASCE, **128**(7), 860-869.
- Dumanoglu, A.A. and Soylik, K. (2003), "A stochastic analysis of long span structures subjected to spatially varying ground motions including the site-response effect", *Eng. Struct.*, **25**(10), 1301-1310.
- Gou, H., Pu, Q., Junming, W., Zeyu, C. and Shiqiang, Q. (2013), "Spatial mechanical behaviors of long-span V-shape rigid frame composite arch bridges", *Struct. Eng. Mech.*, **47**(1), 59-73.
- Gou, H., Pu, Q., Zhou, Y. and Hong, Y. (2015), "Arch-to-beam rigidity analysis for V-shaped rigid frame composite arch bridges", *Steel Compos. Struct.*, **19**(2), 405-416.
- Hao, H. (1998), "A parametric study of the required seating length for bridge decks during earthquake", *Earthq. Eng. Struct. D.*, **27**(1), 91-103.
- Jankowski, R., Wilde, K. and Fujino, Y. (1998), "Pounding of superstructure segments in isolated elevated bridge during earthquakes", *Earthq. Eng. Struct. D.*, **27**(5), 487-502.
- Jeon, J.S., Shafieezadeh, A. and Desroches, R. (2015), "System fragility curves for a long multi-frame bridge under differential support motions", *12th International Conference on Applications of Statistics and Probability in Civil Engineering*, ICASP12 Vancouver, Canada.
- Jia, H.Y.D.X.L. (2018), "Probability analysis method on pounding separation distance of bridges subjected to earthquake excitations", *Eng. Mech.*, **10**(1), 1-9.
- Jia, H., Zhang, D., Zheng, S., Xie, W. and Pandey, M.D. (2013), "Local site effects on a high-pier railway bridge under tridirectional spatial excitations: Nonstationary stochastic analysis", *Soil Dyn. Earthq. Eng.*, **52**, 55-69.
- Kaiming, B. and Hong, H. (2012), "Influence of ground motion spatial variations and local soil conditions on the seismic responses of buried segmented pipelines", *Struct. Eng. Mech.*, **44**(5), 663-680.
- Kawashima, K. and Unjoh, S. (1996), "Impact of Hanshin/Awaji earthquake on seismic design and seismic strengthening of highway bridges", *Struct. Eng. /Earthq. Eng.*, JSCE, **13**(2), 211-240.
- Kawashima, K., Takahashi, Y., Ge, H., Wu, Z. and Zhang, J. (2009), "Reconnaissance report on damage of bridges in 2008 Wenchuan, China, earthquake", *J. Earthq. Eng.*, **13**(7), 965-996.
- Kiureghian, A.D. (1996), "A Coherency model for spatially varying ground", *Earthq. Eng. Eng. Vib.*, **25**(1), 99-111.
- Lin, C.J. and Huang, H.H. (2008), "Reconnaissance report of 0512 China Wenchuan earthquake on bridges", *The 14th World Conference on Earthquake Engineering*, Beijing, China.
- Maison, B.F. and Kasai, K. (1990), "Analysis for type of structural pounding", *J. Struct. Eng.*, ASCE, **116**(4), 957-977.
- Maison, B.F. (1992), "Dynamics of pounding when two buildings collide", *Earthq. Eng. Struct. D.*, **21**(9), 771-786.
- Matasovic, N. "Cyclic characterization of liquefiable sands", *J. Geotech. Eng.*, ASCE, **11**, 1085-1821.
- Penzien, J. (2006), "Seismic ground-motion criteria for bridge design", *The 4th International Conference on New Dimensions in Bridges*, Changsha, China.
- Ruangrassamee, A. and Kawashima, K. (2001), "Relative displacement response spectra with pounding effect", *Earthq. Eng. Struct. D.*, **30**(10), 1511-1538.
- Pacific Earthquake Engineering Research Center, PEER ground motion database. (2005), <http://peer.berkeley.edu/smcat/index.html>
- Sharmin, F., Hussan, M., Kim, D. and Cho, S.G. (2017), "Influence of soil-structure interaction on seismic responses of offshore wind turbine considering earthquake incident angle", *Earthq. Struct.*, **13**(1), 39-51.
- Wang, F., Zhou, Y., Wang, S., Wang, L. and Wei, C. (2010), "Investigation and assessment of seismic geologic hazard triggered by the Yushu earthquake using geo-spatial information technology", *Disast. Adv.*, **3**(4), 72-76.
- Won, J.H., Mha, H.S. and Kim, S.H. (2015), "Effects of the earthquake-induced pounding upon pier motions in the multi-span simply supported steel girder bridge", *Eng. Struct.*, **93**, 1-12.
- Xiao-jun, L.I. and Qing, P.E.N.G. (2001), "Calculation and analysis of earthquake ground motion parameters for different site categories", *Earthq. Eng. Eng. Vib.*, **21**(1), 29-36.
- Yin, X., Fang, Z. and Cai, C.S. (2011), "Lateral vibration of high-pier bridges under moving vehicular loads", *J. Bridge Eng.*, **16**(3), 400-412.
- Yousef, B. and Vitelmo, V.B. (2004), *Earthquake Engineering From Engineering Seismology to Performance-Based Engineering*, CRC Press LLC. New York.
- Zanardo, G., Hao, H. and Modena, C. (2002), "Seismic response of multi-span simply supported bridges to spatially varying earthquake ground motion", *Earthq. Eng. Struct. D.*, **31**(6), 1325-1345.
- Zhang, D., Jia, H., Zheng, S., Xie, W. and Pandey, M.D. (2014), "A highly efficient and accurate stochastic seismic analysis approach for structures under tridirectional nonstationary multiple excitations", *Comput. Struct.*, **145**, 23 - 35.
- Zhao Jingang, D.B.Z.Y. (2017), "Comparison of constitutive concrete models in OpenSees for hysteretic behavior of structures", *J. Guilin Univers. Tech.*, **37**(1), 59-67.